Journal of Energy and Power Engineering 7 (2013)

Influence of DFIG Wind Turbine Protection and Control during Voltage Dip on Circuit Breaker Operation

Anssi Salomo Mäkinen, Ontrei Raipala, Sami Repo and Heikki Tuusa

Department of Electrical Energy Engineering, Tampere University of Technology, Tampere FI-33101, Finland

Received: March 26, 2012 / Accepted: May 22, 2012 / Published: January 31, 2013.

Abstract: This paper analyzes a DFIG (doubly fed induction generator) WT (wind turbine) fault current after a symmetrical network voltage dip. The goal is to identify the factors determining how fast the first zero crossings of the fault current occur. This is an important subject because the fundamental property of the CB (circuit breaker) is that it breaks the current when the current is very near zero. The study was conducted using a hardware-in-the-loop test environment constructed using two real time simulators (dSPACE and RTDS) and a commercial protection relay. It is found that the reactive current injection during a voltage dip demanded by the grid codes enhances the operation of the WT protection because the zero crossings of the currents through CB are attained earlier. In addition, the size of the crowbar resistance has a significant influence on the zero crossings.

Key words: DFIG, reactive current, circuit breaker, loss of mains relay protection.

1. Introduction

Global warming, air pollution and the shortage of fossil energy resources are issues increasing the electricity generation from renewable energy sources. Thus, the penetration of wind generation has increased in many areas to a remarkable level and power system is becoming more dependent on the operation of WT (wind turbines). However, the operation of wind turbines must not endanger power system stability. Thus, power system operators have created grid codes which determine how WTs should operate during grid disturbances [1].

As an example, the grid codes of E.ON Netz regarding symmetrical faults are illustrated in Figs. 1a and 1b [2]. The WTs are not allowed to disconnect if the grid voltage is over the red line in Fig. 1a in order to prevent the cascade tripping of a large number of WTs. In addition, the WTs should be able to inject reactive power into the grid if the grid voltage is depressed, Fig. 1b. The grid codes in Figs. 1a and 1b are meant for wind farm units connected to the high voltage network. However, it is anticipated that similar requirements will be issued for medium voltage network connected wind turbine units as the penetration of wind generation increases.

The DFIG (doubly fed induction generator) WT concept in Fig. 2 consists of a wound rotor induction generator whose stator is directly connected to the grid while the rotor is connected to the grid through a frequency converter. The converter rating is typically one third of the WT nominal power implying small size, costs and losses [1].

1.1 Crowbar Protection of DFIG Wind Turbine

In stationary state, the amplitude of the rotating magnetic flux of the DFIG is proportional to the stator voltage. A symmetrical voltage dip in the stator terminals decreases the amplitude of the rotating flux instantaneously and generates a non-rotating transient flux component. This achieves its maximum value at the beginning of the voltage dip and declines to zero according to the RL transient time constant of the

Corresponding author: Anssi Salomo Mäkinen, research field: Control of wind turbines. E-mail: anssi.makinen@tut.fi.

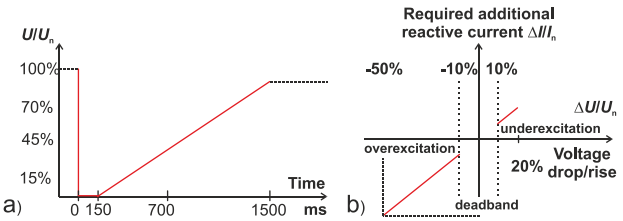

Fig. 1 (a) WT operation limit curve during a voltage dip; (b) voltage support of WT during a fault [2].

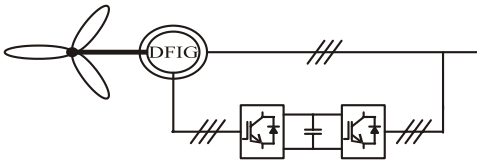

Fig. 2 DFIG WT concept.

stator. The induced voltage to the DFIG rotor is proportional to the stator to rotor turns ratio of the generator and angular slip frequency i.e., the difference between the synchronous angular frequency of the flux and the rotor electrical angular speed. Because the angular frequency of the transient flux component is zero, the transient flux generates very high rotor voltages [3].

A deep network voltage dip induces higher rotor voltages than the RSC (rotor side converter) can generate from the DC-link voltage of the frequency converter. Thus, the RSC can not control the rotor currents and the currents can not be limited [3]. Typically, the RSC is disconnected from the rotor circuit and the crowbar, i.e., a set of resistors, is connected to the rotor circuit in order to decrease the rotor currents and to protect the converter.

The crowbar protection may be either passive or active. Passive crowbar protection is illustrated in Fig. 3. The protection is activated when the thyristor is turned to on-state. The DFIG operates then like an induction generator with increased rotor resistance [4]. The main drawback is that the WT is always disconnected from the grid after crowbar activation and the grid codes are not fulfilled.

In active crowbar protection, the switch based on insulated gate bipolar transistor IGBT or gate turn-off thyristor GTO is used as shown in Fig. 4 [5]. The crowbar can be switched off after the induced rotor voltages have been reduced so much that the rotor

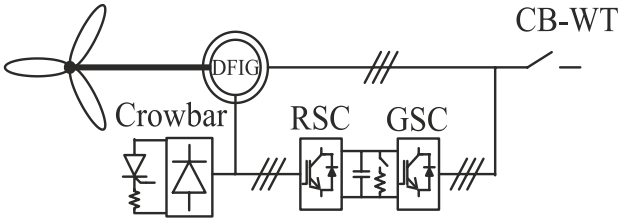

Fig. 3 DFIG with passive crowbar protection [4].

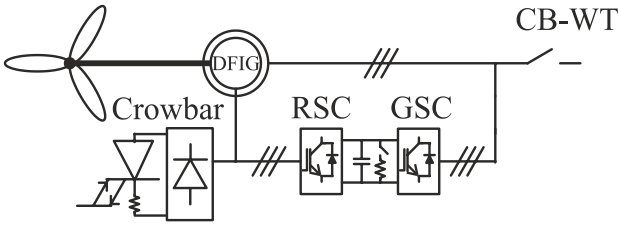

Fig. 4 DFIG with active crowbar protection.

currents can be controlled by using the RSC again. Thus, the WT may survive the voltage dip without disconnection. In addition, the DFIG can inject reactive current into the network during the fault as demanded by the grid codes.

1.2 Relay Protection and Circuit Breaker Operation

The WT units connected to the distribution network are equipped with LOM (loss of mains) protection relay in order to prevent unintentional islanding. Traditionally, the LOM relay detects islanding if the measured grid frequency or connection point voltage exceeds the limits of the relay settings. After that, the relay sends a trip command to the CB (circuit breaker) to disconnect the turbine from the grid.

The appearance of the transient flux after a voltage dip generates DC-component to the DFIG stator currents. Naturally, this DC-component is also presented in the currents flowing through the CB [3]. However, the fundamental property of the CB is that it can interrupt each of the phase currents only near the zero crossings of the currents [6]. In other words, the CB currents do not cross zero, an arc will maintain the current path between the breaker contacts even while the CB attempts to open due to the trip command sent by the relay. This consequently delays the

disconnection of the WT, which can be very harmful for the use of fast AR (automatic reclosing).

The fast AR is meant for removing temporary faults automatically without causing an extended interruption to the power supply. This is done by briefly opening the feeder CB connecting the faulted feeder to the supplying network, usually from 0.2 s to a couple of seconds. In the case of a temporary fault, the fault arc usually extinguishes during this short de-energized period. The majority of faults on overhead lines are temporary in nature and thus clearable with the help of the fast AR [7]. However, it is necessary for all the generating units connected to the faulted feeder to be disconnected during the open time of the feeder CB. Otherwise, the generating units would maintain the voltage at the fault location and would prolong arc extinction causing the AR sequence to fail. Even short delays in the disconnection of the generating units can cause the AR sequences to fail. Moreover, out-of-phase reclosing causing dangerous stresses to the generating unit may occur if the disconnection of the generating unit is delayed considerably [8].

1.3 Purpose of the Study

In this paper, two different DFIG WT operation methods during symmetrical voltage dips are compared and their fault current responses analyzed. The first method uses passive crowbar protection and the second method uses active crowbar protection with the reactive current injection demanded by the grid codes. The aim is to identify the factors determining the instant of first zero crossing in the fault current which has an impact on the operation of the CB. It is shown that reactive current injection during a voltage dip has a great impact on the zero crossings. In addition, the size of the crowbar resistance is of considerable importance.

2. System Modeling

The space-vector based equivalent circuit of the modelled DFIG is presented in Fig. 5 [9]. The transformer inside the induction generator block describes the rotor to stator turns ratio, N, of the generator, where N_s and N_r are the number of turns of

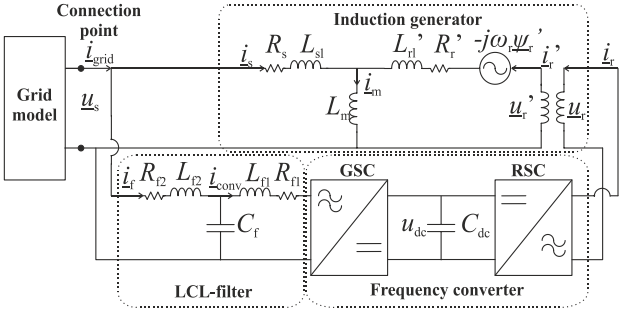

Fig. 5 Equivalent circuit of the DFIG

stator and rotor, respectively. The variables with the superscript are reduced to the stator as follows:

$$L_{rl}' = \left(\frac{N_s}{N_r}\right)^2 L_{rl} = \left(\frac{1}{N}\right)^2 L_{rl} \quad (1)$$

$$R_r' = \left(\frac{1}{N}\right)^2 R_r \quad (2)$$

$$\underline{i}_r' = N\underline{i}_r \quad (3)$$

$$\underline{u}_r' = \frac{1}{N}\underline{u}_r \quad (4)$$

where L_{sl} and L_{rl}' are the leakage inductances of the stator and the rotor, respectively. R_s and R_r are the stator and rotor resistances, respectively.

The voltage equations of the DFIG can be expressed in a synchronous reference frame that is oriented to the network voltage vector as follows:

$$\underline{u}_s = R_s\underline{i}_s + \frac{d\underline{\psi}_s}{dt} + j\omega_s\underline{\psi}_s \quad (5)$$

$$\underline{u}_r = R_r'\underline{i}_r' + \frac{d\underline{\psi}_r'}{dt} + j(\omega_s - \omega_r)\underline{\psi}_r' \quad (6)$$

where $\underline{u}$, $\underline{i}$, $\underline{\psi}$ and R corresponds to the voltage vector, current vector, flux linkage vector and resistance, respectively. Subscripts *s* and *r* correspond to the stator and rotor respectively. The synchronous angular frequency of the grid voltage is ω_s and the electrical angular frequency of the rotor is ω_r.

The flux linkage space vectors are:

$$\underline{\psi}_s = L_s\underline{i}_s + L_m\underline{i}_r' \quad (7)$$

$$\underline{\psi}_r' = L_r'\underline{i}_r' + L_m\underline{i}_s \quad (8)$$

where L_s and L_r corresponds to the stator and rotor self inductances and L_m is the magnetizing inductance.

The self-inductances are defined as $L_s = L_{sl} + L_m$ and $L_r' = L_{rl}' + L_m$.

Stator and rotor coupling factors k_s and k_r as well as the leakage factor σ are used to simplify the equations and are defined as [9]:

$$k_s = \frac{L_m}{L_s} \tag{9}$$

$$k_r = \frac{L_m}{L_r'} \tag{10}$$

$$\sigma = 1 - \frac{L_m^2}{L_s L_r'} \tag{11}$$

The stator and the rotor current vectors can be calculated using Eqs. (7)-(11):

$$\underline{i}_s = \frac{\underline{\psi}_s}{\sigma L_s} - k_r \frac{\underline{\psi}_r'}{\sigma L_s} \tag{12}$$

$$\underline{i}_r' = \frac{\underline{\psi}_r'}{\sigma L_r'} - k_s \frac{\underline{\psi}_s}{\sigma L_r'} \tag{13}$$

The parameters of the generator, DC-link capacitor, inductor-capacitor-inductor LCL-filter and transformer are presented in Table 1. Both the RSC (rotor side converter) and the GSC (grid side converter) are assumed to operate in the linear modulation area. In addition, both converters are assumed to execute their voltage reference ideally i.e., the switching performance is not modeled in order to save calculation resources. The transformer saturation is not taken into account.

The grid model is presented in Fig. 6. The distribution network model used in the simulations is a simplified model of a real Finnish distribution network. The model consists of two radial feeders, which are fed by a 16 MVA rated 110 kV/21 kV transformer. The WT is connected to the network through a circuit-breaker controlled by a commercial protection relay. The CB is modeled such that the current path on each phase is interrupted only when the currents crosses the zero.

3. Operation of Induction Generator during Network Fault

The fault current of the induction generator is analyzed in this section. When a three-phase voltage dip occurs at the stator terminals of the DFIG, the crowbar needs to be activated. Thus, the DFIG behaves like an induction generator with increased rotor resistance. Next, the response of the induction generator to the voltage dip on the stator terminals is analyzed. In order to simplify the analysis, the following assumptions are made [10]:

Table 1 Parameters of DFIG and transformer.

Parameter	Value	Parameter	Value
P_n	1,700 kW	L_m	3.8 mH
$u_{s\_line\text{-}to\text{-}line}$	690 V	Turns ratio N	2.73
R_s	0.0027 Ω	Pole pairs	2
L_s	0.089 mH	u_{dc}^{ref}	1,100 V
R_r	0.0026 Ω	C_{dc}	22 mF
L_r	0.092 mH	L_{f1}	190 µH
R_{f1}	15 mΩ	L_{f2}	125 µH
R_{f2}	5 mΩ	C_f	70 µF
Transf. S_n	1.75 MVA	Transf. X_k	6%
Transf. R_k	1%		

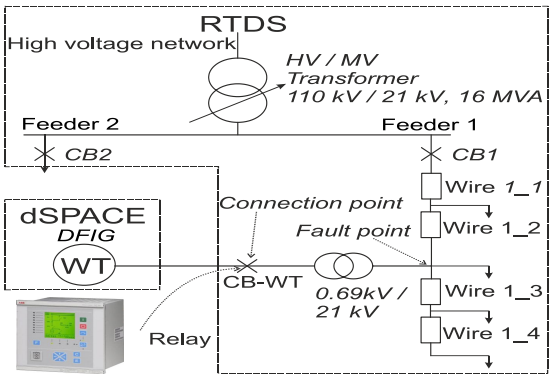

Fig. 6 Grid model.

- generator is idle running ($\omega_r = \omega_s$);
- rotor current is zero before fault ($\underline{i}_r = 0$);
- steady state operation before the fault;
- resistances are ignored before the fault.

The stator voltage vector (Eq. (5)) after simplifications can be expressed as:

$$\underline{u}_s = j\omega_s \underline{\psi}_s = j\omega_s \left(L_s \underline{i}_s + L_m \underline{i}_r' \right) = j\omega_s L_s \underline{i}_s \tag{14}$$

Thus, the stator current vector is:

$$\underline{i}_s = \frac{\underline{u}_s}{j\omega_s L_s} \tag{15}$$

The pre-fault stator and rotor flux linkage vectors are:

$$\underline{\psi}_s = L_s \underline{i}_s + L_m \underline{i}_r' = L_s \underline{i}_s = \frac{\underline{u}_s}{j\omega_s} \tag{16}$$

$$\underline{\psi}_{\mathrm{r}}' = L_{\mathrm{r}}'\underline{i}_{\mathrm{r}}' + L_{\mathrm{m}}\underline{i}_{\mathrm{s}} = L_{\mathrm{m}}\underline{i}_{\mathrm{s}} = \frac{L_{\mathrm{m}}}{L_{\mathrm{s}}}\frac{\underline{u}_{\mathrm{s}}}{j\omega_{\mathrm{s}}} = k_{\mathrm{s}}\frac{\underline{u}_{\mathrm{s}}}{j\omega_{\mathrm{s}}} \quad (17)$$

According to the theorem of constant flux linkage, the flux linkage in both stator and rotor windings remains constant after short-circuit [11]. Thus, the stator and rotor flux linkage vectors in Eqs. (16) and (17) can be used as initial values when calculating the fault current. After the fault, the generator rotor continues to rotate with the angular speed of ω_{s} with respect to the stator. Thus, the rotor flux linkage vector rotates with respect to stator flux linkage with the same speed. Hence, when the resistances are neglected, the post-fault stator and rotor flux linkage vectors in a stator flux reference frame are [10]:

$$\underline{\psi}_{\mathrm{s}} = \frac{U_{\mathrm{s},0}}{j\omega_{\mathrm{s}}} \quad (18)$$

$$\underline{\psi}_{\mathrm{r}}' = k_{\mathrm{s}}\frac{U_{\mathrm{s},0}}{j\omega_{\mathrm{s}}}e^{j\omega_{\mathrm{s}}t} \quad (19)$$

where $U_{s,0}$, is the magnitude of the stator voltage space vector when voltage dip occurs.

The post-fault stator and rotor current vectors can be calculated using Eqs. (12), (13), (18) and (19):

$$\underline{i}_{\mathrm{s}} = \frac{\underline{\psi}_{\mathrm{s}}}{\sigma L_{\mathrm{s}}} - k_{\mathrm{r}}\frac{\underline{\psi}_{\mathrm{r}}'}{\sigma L_{\mathrm{s}}} = \frac{U_{\mathrm{s},0}}{j\omega_{\mathrm{s}}\sigma L_{\mathrm{s}}}\left(1 - k_{\mathrm{r}}k_{\mathrm{s}}e^{j\omega_{\mathrm{s}}t}\right) \quad (20)$$

$$\underline{i}_{\mathrm{r}}' = \frac{\underline{\psi}_{\mathrm{r}}'}{\sigma L_{\mathrm{r}}'} - k_{\mathrm{s}}\frac{\underline{\psi}_{\mathrm{s}}}{\sigma L_{\mathrm{r}}'} = \frac{k_{\mathrm{s}}U_{\mathrm{s},0}}{j\omega_{\mathrm{s}}\sigma L_{\mathrm{r}}'}\left(-1 + e^{j\omega_{\mathrm{s}}t}\right) \quad (21)$$

It can be seen from Eqs. (20) and (21) that the stator and the rotor currents consist of DC- and AC-components. The DC-component appears because the flux linkage in both windings stays constant. As the rotor rotates with respect to the stator, the DC-component in the rotor current generates AC-component to the stator currents. Naturally, the rotor AC-component is generated due to the presence of the stator DC-component and the relative movement between the windings. The frequency of the AC-component is determined by the speed of the generator rotor.

The resistances of the system are not taken into account in the currents in Eqs. (20) and (21). In reality, the resistances damp the DC-component from the currents. The damping is taken into account by using damping factors which describe how fast the DC-component disappears from the currents and they are defined as [10]:

$$T_{\mathrm{s}\sigma} = \frac{\sigma L_{\mathrm{s}}}{R_{\mathrm{s}}} \quad (22)$$

$$T_{\mathrm{r}\sigma} = \frac{\sigma L_{\mathrm{r}}'}{R_{\mathrm{r}}' + R_{\mathrm{crow}}'} \quad (23)$$

where $T_{s\sigma}$ is transient time constant of the stator, $T_{r\sigma}$ is the transient time constant of the rotor and R_{crow} is the crowbar resistance.

The $T_{s\sigma}$ is determined by the machine parameters. The stator current DC component declines faster if σL_s is small or R_s is large. Thus, the trend to design generators with low losses tends to increase the $T_{s\sigma}$. The rotor transient inductance, the rotor resistance as well as the crowbar resistance determine the $T_{r\sigma}$. The selection of R_{crow} has significant influence on the rotor transient time constant. The larger the total rotor resistance, the faster the DC-component disappears from the rotor current. As mentioned above, the rotor current DC-component creates AC-component to the stator current. Thus, if the $T_{r\sigma}$ is small, the AC-component on the stator current disappears quickly.

The damping factors defined in Eqs. (22) and (23) are included in Eqs. (20) and (21) in order to achieve equations for the stator and the rotor currents during a fault:

$$\underline{i}_{\mathrm{s}} = \frac{U_{\mathrm{s},0}}{j\omega_{\mathrm{s}}\sigma L_{\mathrm{s}}}\left[e^{-\frac{t}{T_{\mathrm{s}\sigma}}} - k_{\mathrm{r}}k_{\mathrm{s}}e^{j\omega_{\mathrm{s}}t}e^{-\frac{t}{T_{\mathrm{r}\sigma}}}\right] \quad (24)$$

$$\underline{i}_{\mathrm{r}}' = \frac{U_{\mathrm{s},0}\,k_{\mathrm{s}}}{j\omega_{\mathrm{s}}\sigma L_{\mathrm{r}}'}\left[e^{j\omega_{\mathrm{s}}t}e^{-\frac{t}{T_{\mathrm{s}\sigma}}} - e^{-\frac{t}{T_{\mathrm{r}\sigma}}}\right] \quad (25)$$

Initial values in (24) and (25) were calculated under the assumption that the stator and the rotor resistances are zero. After connection of the crowbar resistance to the rotor circuit the assumption is no longer correct. The impact of crowbar resistance on the stator current initial value was calculated in Ref. [10] as follows:

$$\underline{i}_{\mathrm{s}} = \frac{U_{\mathrm{s},0}}{\sqrt{\left(\left(j\omega_{\mathrm{s}}\sigma L_{\mathrm{s}}\right)^2 + R_{\mathrm{crow}}'^2\right)}}\left[e^{-\frac{t}{T_{\mathrm{s}\sigma}}} - k_{\mathrm{r}}k_{\mathrm{s}}e^{j\omega_{\mathrm{s}}t}e^{-\frac{t}{T_{\mathrm{r}\sigma}}}\right] \quad (26)$$

4. Control System

The control system of the WT consists of three parts. The control system of the GSC controls the DC-link voltage to a constant value. The control system of the RSC adjusts the speed of the WT and contributes to the grid voltage control by controlling the reactive power exchange with the grid. The GSC is also able to control its reactive current output. The pitch control system is used to curtail wind power production during high wind speeds in order to reduce the load of the mechanical and electrical parts of the turbine. The pitch control system used is presented in Ref. [12].

4.1 Control System of Grid Side Converter

The GSC control is done in the reference frame oriented to the positive sequence component of the connection point voltage vector $\underline{u}_s$. The positive sequence component of the voltage is detected using a DSOGI-FLL (dual second order generalized integrator-frequency-locked loop), Fig. 7 [13]. The DSOGI is a bandpass filter. The outputs are u_α' and u_β', which are the filtered versions of the grid voltage components in the stationary reference frame, as well as qu_α' and qu_β', which are the 90° shifted versions of u_α' and u_β', respectively. The output signals are used to calculate PNS (the positive and the negative sequence) components of the grid voltage vector. The PNS components can be estimated accurately as long as the filter resonance frequency ω' corresponds to the grid frequency. Because the grid frequency is not constant, the FLL is used to modify the filter resonance frequency to correspond to the grid frequency.

The control system of the GSC is illustrated in Fig. 8. The DC-link voltage controller maintains constant DC-link voltage u_{dc}, thereby ensuring the active power balance between the RSC and the GSC. The output of the controller is the reference of the converter current vector x-component $i_{conv,x}$*.

In normal operation, the reference of the converter current y-component $i_{conv,y}$* is set at zero and the GSC does not control the reactive power. However, when the network voltage dip is sensed by the fault control block, the current reference is modified in order to

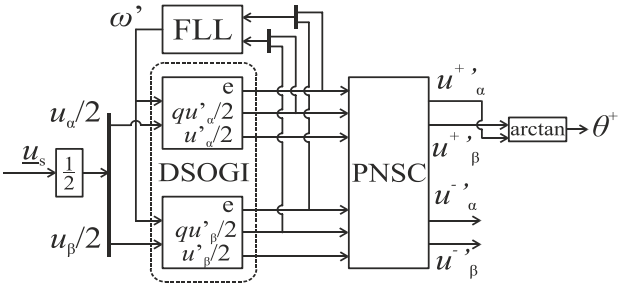

Fig. 7 Schematic diagram of DSOGI-FLL [13].

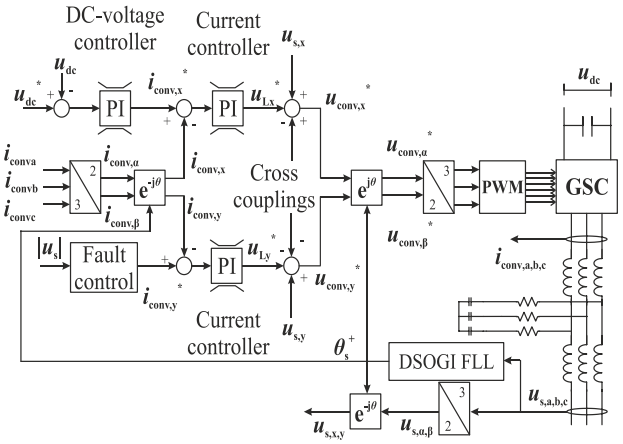

Fig. 8 Control of grid side converter.

feed reactive power to the grid. The output of the control system is the reference for converter voltage vector $\underline{u}_{conv}$* [14].

4.2 Control System of Rotor Side Converter

The control system of the RSC is illustrated in Fig. 9. The control is based on the vector control in a reference frame that is oriented to the estimated positive sequence component of the stator flux linkage vector. The stator flux linkage is first calculated from the measured stator voltages and currents. The PNS components of the stator flux linkage are then estimated using the DSOGI-FLL.

The RSC is controlled so that the DFIG extracts the maximum power from the wind by producing a torque that optimizes the ratio between the blade tip speed

and the wind speed. The output of the speed controller is the reference for the torque t_e^*. The torque controller gives the reference value for the rotor current y-component i_{ry}*. The reactive power controller controls the reactive power exchange with

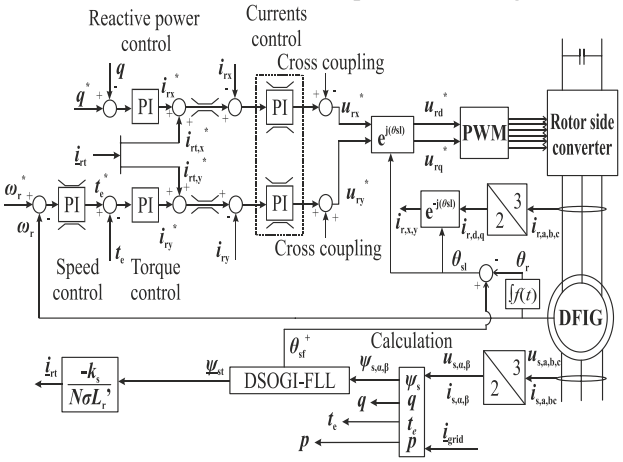

Fig. 9 Control of rotor side converter.

the grid and it gives the reference for the rotor current *x*-component i_{rx}*. The cross coupling compensation terms are added to the output of the current controller and the reference for rotor converter voltage components u_{rd}* and u_{rq}* are achieved.

4.3 Transient Flux Compensation Control

As mentioned before, the non-rotating transient flux generates very high rotor voltages. In transient flux compensation control the effect of transient flux is minimized by generating rotor current component that opposes the transient flux. After the transient flux is removed, all current capacity of the RSC can be utilized for reactive current injection which is desirable according to grid codes [15].

The transient flux compensation current component is calculated as follows. The DSOGI-FLL is used to calculate the positive sequence component from the stator flux. In the case of symmetrical voltage dip, the transient flux linkage vector $\underline{\psi}_{st}$ is the difference between the total stator flux linkage vector $\underline{\psi}_s$ and the positive sequence component of the flux linkage vector $\underline{\psi}_{s+}$ [16].

$$\underline{\psi}_{\mathrm{st}} = \underline{\psi}_{\mathrm{s}} - \underline{\psi}_{\mathrm{s+}} \tag{27}$$

The rotor flux linkage vector can be solved from Eq. (13) [16]:

$$\underline{\psi}_{\mathrm{r}}' = k_{\mathrm{s}}\underline{\psi}_{\mathrm{s}} + \sigma L_{\mathrm{r}}'\underline{i}_{\mathrm{r}}' \tag{28}$$

The rotor flux linkage vector as well as the rotor current vector can be decomposed into two vectors consisting of positive sequence components and the transient components.

$$\underline{\psi}_{\mathrm{r+}}' + \underline{\psi}_{\mathrm{rt}}' = k_{\mathrm{s}}\left(\underline{\psi}_{\mathrm{s+}} + \underline{\psi}_{\mathrm{st}}\right) + \sigma L_{\mathrm{r}}'\left(\underline{i}_{\mathrm{r+}}' + \underline{i}_{\mathrm{rt}}'\right) \tag{29}$$

where $\underline{\psi}_{r+}$ and $\underline{i}_{r+}$ are the positive sequence components of the rotor flux linkage vector and the rotor current vector. The $\underline{\psi}_{rt}$ and the $\underline{i}_{rt}$ are the transient terms. In transient flux compensation, the aim is to minimize the impact of the transient flux on the rotor. Thus, the transient rotor flux linkage vector $\underline{\psi}_{rt}'$ in Eq. (29) is set at zero.

$$\underline{\psi}_{\mathrm{rt}}' = k_{\mathrm{s}}\underline{\psi}_{\mathrm{st}} + \sigma L_{\mathrm{r}}'\underline{i}_{\mathrm{rt}}' = 0 \tag{30}$$

The rotor current vector used to cancel the transient flux, can be calculated from Eq. (30) [16]:

$$\underline{i}_{\mathrm{rt}} = \frac{\underline{i}_{\mathrm{rt}}'}{N} = -\frac{k_{\mathrm{s}}}{N\sigma L_{\mathrm{r}}'}\underline{\psi}_{\mathrm{st}} = -\frac{k_{\mathrm{s}}}{N\sigma L_{\mathrm{r}}'}\left(\underline{\psi}_{\mathrm{s}} - \underline{\psi}_{\mathrm{s+}}\right) \tag{31}$$

4.4 FRT Method for DFIG Wind Turbine

The FRT (fault ride through) method used in this study is presented in this section. The method uses active crowbar protection, Fig. 4, transient flux compensation and reactive current injection to the network as demanded by the grid codes [16, 17].

As a result of a deep network voltage dip, high and uncontrolled rotor currents start to flow. When the rotor currents exceed the current capacity of the RSC, the crowbar protection is activated and the RSC stops modulation. As a consequence, the rotor currents start to decrease. After the rotor currents have decreased below the current capacity of the RSC, the crowbar is deactivated and the RSC is activated. The transient flux compensation current components $i_{rtx,y}$ calculated in Eq. (31) are set as a reference for the current controllers as shown in Fig. 9. As the transient flux declines, the current needed to cancel the transient flux decreases. When the magnitude of the calculated compensation current vector $|\underline{i}_{rt}|$ is smaller than the

current capacity of the RSC, the rest of the capacity is utilized for reactive current injection to the grid. Thus, the current references during a voltage dip are:

$$i_{\mathrm{rt,x}}{}^{*} = -\frac{k_{\mathrm{s}}}{N\sigma L_{\mathrm{r}}{}'}\psi_{\mathrm{st,x}} \tag{32}$$

$$i_{\mathrm{rt,y}}{}^{*} = -\frac{k_{\mathrm{s}}}{N\sigma L_{\mathrm{r}}{}'}\psi_{\mathrm{st,y}} \tag{33}$$

$$i_{\mathrm{rx}}{}^{*} = \sqrt{\left(i_{\mathrm{r\,max}}\right)^2 - \left(\left|\underline{i}_{\mathrm{rt}}{}^{*}\right|\right)^2} \tag{34}$$

$$i_{\mathrm{ry}}{}^{*} = 0 \tag{35}$$

where i_{rmax} is the current capacity of the RSC and $|\underline{i}_{rt}{}^{*}|$ is the magnitude of the transient current vector. After the transient flux is cancelled, the current $\underline{i}_{rt}$ is zero and the whole current capacity of the RSC is utilized for the reactive power injection.

The GSC also starts to feed reactive current to the network immediately after the fault control block senses the voltage dip. The x-axis current is prioritized in order to keep the DC-link voltage at the desired value. However, the difference between the GSC current capacity and the x-axis current is set as the reference to the y-axis current component in Fig. 8.

Every time the WT senses the deep voltage dip on the network it immediately starts to execute its FRT process. The decision whether or not the turbine should be disconnected from the grid is determined by the WT LOM protection relay. If the LOM relay sends the trip command, the WT is disconnected from the grid as a result of the CB opening and both the RSC and the GSC cease modulation.

5. Experimental Test Setup

The study is conducted using the hardware-in-the-loop test setup shown in Fig. 10. The test setup consists of a dSPACE DS1103 controller board, a RTDS (real-time digital simulator), a REF 543 relay by ABB and an Omicron CMS 156 amplifier. The RTDS is used to simulate the power system model while the WT model is simulated using the dSPACE, Fig. 6 [12, 18].

5.1 Practical Implementation

The block diagram of the RTDS/dSPACE implementation is shown in Fig. 11. The dSPACE simulates in real time the operation of the DFIG, which is modeled in Simulink. The ControlDesk program is used to control and observe the simulation. The power

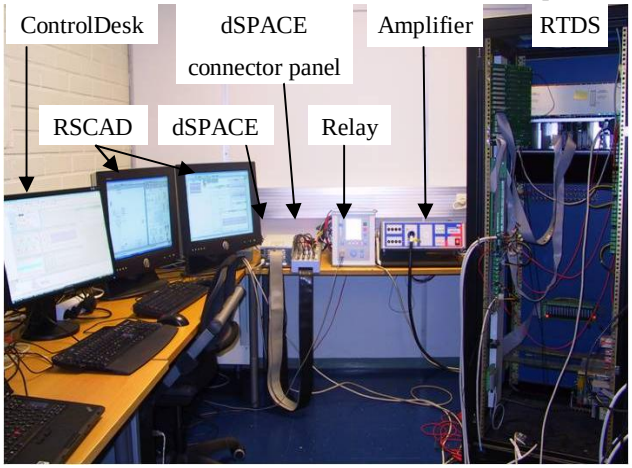

Fig. 10 Hardware-in-the-loop test setup.

system model is created in the RSCAD Draft mode. The RSCAD Runtime mode is used to control the real time simulation performed by the RTDS. The data transmission between the real time simulators is done through analog signals. In other words, first the digital signals of the simulator are converted into analog signals, which are converted back to digital signals when fed to the other simulator. The dSPACE receives the connection point voltages $u_{s(a,b,c)}$, an interruption signal *int* and the information on whether the relay is open or closed, *relay on*, from the RTDS and gives the connection point current $i_{grid(\alpha,\beta)}$ back. From the RTDS viewpoint, the WT is modeled as a current source. The interruption signal *int* is used to synchronize the calculations of the dSPACE and the RTDS. The transformer secondary side voltage measurement, i.e., the connection point voltage, is fed from the RTDS to the relay via an amplifier. The amplifier is needed since the voltage of the signals provided from the RTDS digital to analog converter card is not sufficient for the relay [18].

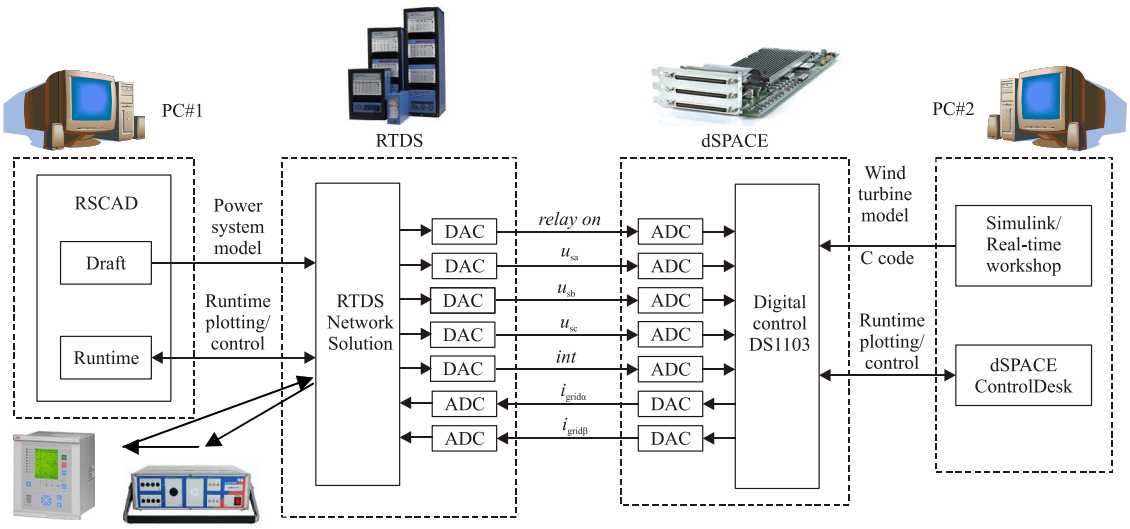

Fig. 11 Practical implementation of the research environment.

6. Simulation Results

In this section, two operation methods of the DFIG during symmetrical voltage dip are compared and fault current responses are analyzed. In addition, the impact of the crowbar resistance selection on the fault current zero crossings is evaluated. In the first method, the DFIG protection relies on the passive crowbar protection and no reactive current is fed into the network. The second method uses the fault ride through (FRT) strategy described in Section 4.4. The purpose is to show the existence of the interactions between the control and protection of the DFIG and the fault current zero crossings.

A three-phase short circuit occurring on the primary side of the WT transformer in Fig. 6, is simulated. This is modeled as the three phase voltage dip on the fault point which lasts 250 ms. This is comparable to the real case where the feeder overcurrent protection opens the feeder circuit breaker CB1 after 50 ms from the beginning of the fault and the feeder CB1 is automatically reclosed 200 ms after being opened. The real feeder overcurrent protection relay and its automatic reclosing function were not included in the simulations due to the lack of the real feeder relay. The crowbar resistance is 0.4 pu in both methods. The interest is in whether or not the DC component in the DFIG fault current disturbs this very fast AR sequence.

In the case where the first method is used, a three-phase voltage dip occurs at the connection point at 7.5 s as shown in Fig. 12a. The voltage dip induces high rotor voltages due to the transient flux and the currents in the rotor windings increase. The passive crowbar is activated when the peak value of the rotor current exceeds the current capacity of the RSC, which in this case is 900 A rms (peak value 1,270 A). The rotor currents and the crowbar activation are shown in Fig. 13a. The passive crowbar remains connected as long as the currents flow in the rotor circuit. The frequency of the rotor current corresponds to the angular slip frequency. During the voltage dip the non-rotating transient flux causes the rotor current frequency to increase.

The LOM protection relay senses very low connection point voltage and after 200 ms from the beginning of the fault it sends a trip command to open the WT CB. The currents through the CB are shown in Fig. 14a. It can be seen that the DC-component caused by the transient flux appears in the currents. In addition, before the time 7.54 s, AC-component is also superimposed to the currents. The AC-component appears due to the DC-component in the rotor currents.

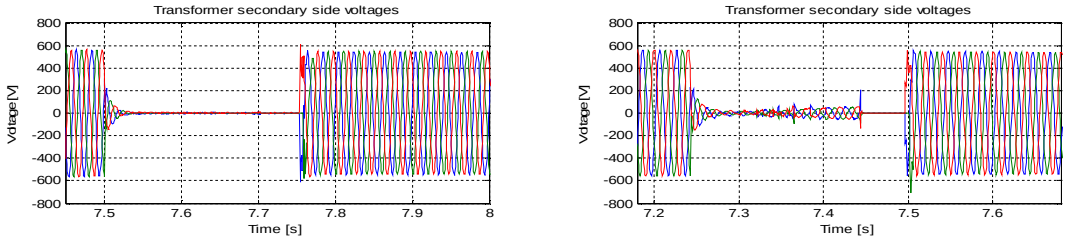

(a) (b)

Fig. 12 Connection point voltage: (a) without reactive current injection; (b) with reactive current injection.

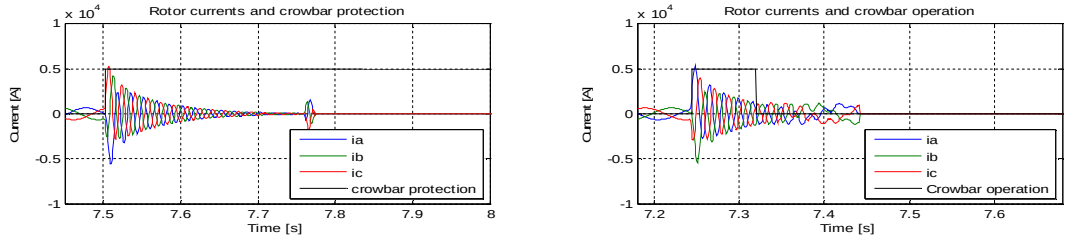

(a) (b)

Fig. 13 Rotor current and crowbar operation: (a) without reactive current injection; (b) with reactive current injection.

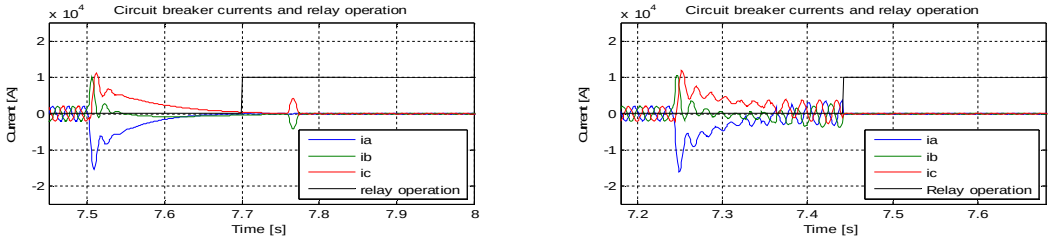

(a) (b)

Fig. 14 CB current and relay operation: (a) without reactive current injection; (b) with reactive current injection.

The DC-component in rotor currents declines according to the transient time constant of the rotor (Eq. (23)). After the DC-component has disappeared from the rotor currents, the second term in brackets in Eq. (24) becomes negligible and the CB currents do not contain AC-component. Although the LOM relay sends a trip command, the CB can not interrupt the currents due to the absence of the currents' zero crossings. In this case the CB currents are not zero when the automatic reclosing occurs 250 ms after the beginning of the fault. The AR therefore fails. In reality, the voltages can not be restored to the WT connection point due to the failed AR. However, the voltages appear in Fig. 12a because the AR sequence is modeled as the three phase voltage dip in the fault point which lasts 250 ms and the real operation of feeder CB is not modeled.

In the second method, the FRT strategy of Section 4.4 is used. The identical connection point voltage dip compared to the previous case occurred at 7.24 s, as shown in Fig. 12b. The fault increases the rotor currents and crowbar protection is activated as shown in Fig. 13b. The crowbar is turned off at 7.32 s.

The CB currents and the LOM relay operation are shown in Fig. 14b. During the time when the crowbar is activated the CB current has a greater AC-component than in Fig. 14a. This AC-component is caused by the reactive current fed by the GSC. The current capacity of GSC was selected to be 600 A rms (peak value 848 A).

When the crowbar is turned off, the AC oscillations are increased further due to the injection of reactive current from both the GSC and the RSC. Due to these oscillations the currents' zero crossings on each phase

are attained earlier. Hence, the CB is able to break the currents as the LOM relay sends the trip command at 7.44 s. In this case, the CB could even disconnect the turbine from the grid much earlier. However, the time of disconnection is determined by the settings of the LOM protection relay.

6.1 Effect of Crowbar Resistance

In the following simulations, the crowbar resistance is 0.05 pu. Otherwise, the simulations are identical to the case above. In the first case, passive crowbar protection is used. The connection point voltage dips at 7.57 s as shown in Fig. 15a. The rotor currents are higher than in the situation where higher crowbar resistance value was used as shown in Fig. 16a. The peak value of the rotor current is approximately 7,500 A, while in the previous case the maximum peak current was approximately 5,200 A. It should be noted that the rotor voltages are lower during the crowbar connection due to the lower crowbar resistance.

The CB currents and the LOM relay operation are shown in Fig. 17a. The CB currents are higher when the low crowbar resistance is used as expected based on Eq. (26). The peak value of the currents is slightly less than 21 kA as in the previous case the corresponding value is about 16 kA. The remarkable AC-component appears because the transient time constant of the rotor (Eq. (23)) has increased significantly as the crowbar resistance decreases. Thus, the slowly declining rotor DC-component generates the AC-component to the stator currents as seen also in Eq. (24). Due to the significant AC-component the currents' zero crossings are attained early and the AR sequence is successful.

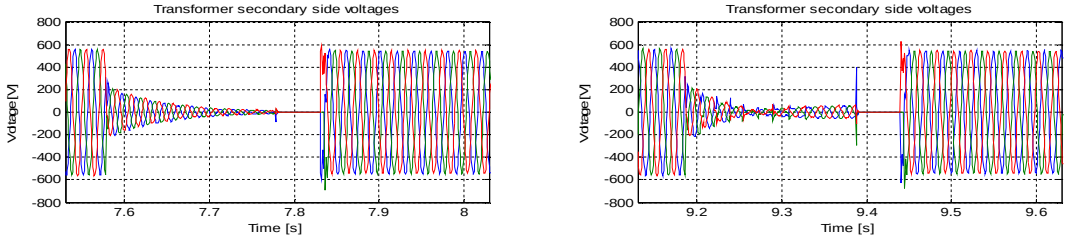

(a) (b)

Fig. 15 Connection point voltage: (a) without reactive current injection, (b) with reactive current injection.

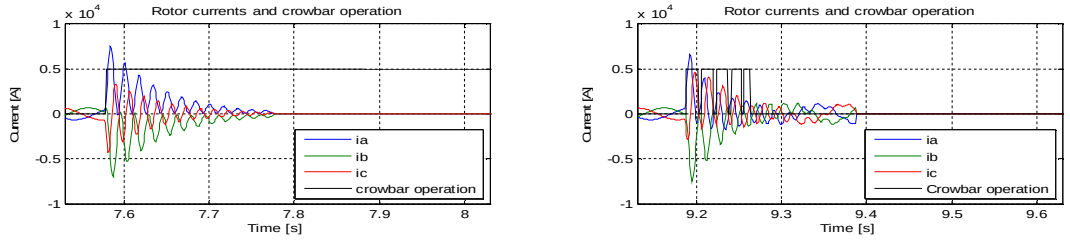

(a) (b)

Fig. 16 Rotor current and crowbar operation: (a) without reactive current injection; (b) with reactive current injection.

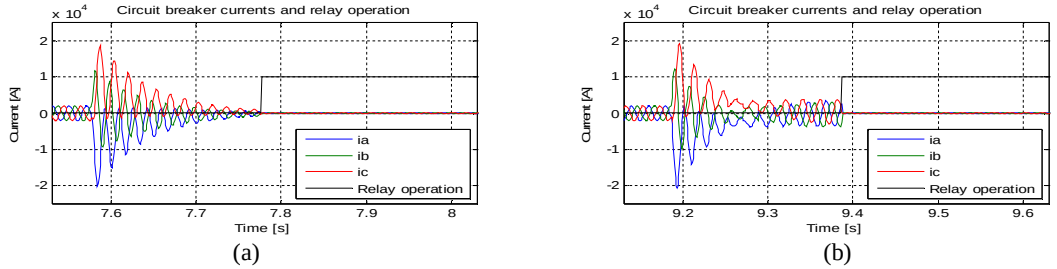

(a) (b)

Fig. 17 CB current and relay operation: (a) without reactive current injection; (b) with reactive current injection.

The connection point voltage when the second method is used is shown in Fig. 15b. Low crowbar resistance causes the rotor currents to decrease rapidly, which deactivates the crowbar and activates the RSC as shown in Fig. 16b. However, when the RSC is reconnected, the rotor currents again increase over the limit causing the crowbar to re-activate. This is because the transient flux has not yet disappeared and due to the flux the current oscillates around its reference. Repetitive crowbar activation could be avoided, for example, by increasing the crowbar connection time [16].

The zero crossings of the CB currents are attained earlier than the LOM relay operates, Fig. 17b. Thus, the CB can disconnect the WT without problems in both the passive and the active crowbar cases.

7. Discussion

In the simulation model, the operation of the CB is modeled such that the current path is interrupted only as the current crosses zero. However, the resistance of the fault arc was not taken into account and in that sense the simulation results represent the worst case scenario. In reality, and especially at medium voltage levels, the zero crossings of the currents will be attained earlier due to the arc resistance. However, the effect of the fault arc resistance on the zero crossings of the currents decreases as the WT connection point voltage level increases [6].

Although the resistance of the arc in the medium voltage network accelerates the zero crossings, even a short delay in the disconnection of the generating units may cause problems when using fast AR. Actually, it is not even enough that the arc is fully extinguished before the feeder breaker reclosing. Without sufficient time delay to allow the ionized gas created by the fault arc to disperse, the arc will start conducting again after the AR. Thus, the fast AR will fail [19]. Consequently, it is vital that the CB currents crosses zero quickly after the LOM relay has sent the trip command.

If expensive communication based LOM protection is used, the feeder relay sends a trip command to the LOM relay. The signal transfer time between the relays may be less than 30 ms [20]. The almost simultaneous operation of the relays is highly desirable from the power system protection and fast AR viewpoints because of the reliable protection against islanding and the avoidance of failed reclosing [21]. However, the very fast operation of the LOM relay forces the DFIG CB to interrupt the current, which contains a significant DC component.

It should be noted that every time the CB attempts to interrupt direct current the arc will cause additional stresses on the CB, thereby shortening its lifetime. In addition, too long an arc may destroy the CB. The arcing time depends not only on the voltage level of the generator connection but also on the resistance and reactance in the fault path. The trend to design generators and the transformers with minimized losses decreases the resistance and thus delays the current zero crossings when the fault occurs near the generator. If the distance between the generator and the fault point is large due to the increased resistance in the fault path, the stator current DC component disappears quickly, as indicated by Eq. (22) and zero crossings are achieved early [6].

8. Conclusions

This paper analyzes the DFIG wind turbine fault current after a symmetrical network voltage dip. After the voltage dip, the stator currents of the DFIG contain a DC-component which delays the zero crossings of the currents that flow through the CB (circuit breaker). However, the CB can interrupt the currents only when the currents are very near to zero. Thus, the subject is important as regards protection. The study was conducted utilizing the real-time simulation environment with relay-in-the-loop.

The grid codes nowadays insist that WTs should inject reactive current into the grid during a voltage dip. The simulation results show that the reactive current

injection adds AC-component to the CB currents. Also, the selection of low crowbar resistance increases the current AC-component. The AC-component accelerates zero crossings of the grid current, which improves the current breaking of the WT CB.

References

[1] T. Ackermann, Wind Power in Power System, John Wiley & Sons, Ltd., Royal Institute of Technology, Stockholm, Sweden, 2005.

[2] E.ON Netz GmbH, Grid code—High and extra high voltage, Apr. 2006.

[3] J. Lopez, P. Sanchis, X. Roboam, L. Marroyo, Dynamic behavior of the doubly fed induction generator during three phase voltage dips, IEEE Transactions on Energy Conversion 22 (3) (2007) 709-717.

[4] Z. Chen, J. Guerrero, F. Blaabjerg, A review of the state of the art of power electronics for wind turbines, IEEE Transactions on Power Electronics 24 (8) (2009) 1859-1875.

[5] S. Seman, J. Niiranen, A. Arkkio, Ride-through analysis of doubly fed induction wind-power generator under unsymmetrical network disturbance, IEEE Transactions on Power Systems 21 (4) (2006) 1782-1789.

[6] J. Gallagher, N. McDonagh, W. Phang, The effect of delayed zero crossings following a short circuit on system stability, in: GCC Power 2010 Conference, Ritz-Carlton, Doha, Qatar, p. 6.

[7] I.D. Kim, H.S. Cho, J.K. Park, A variable dead time circuit breaker auto-reclosing scheme using artificial neural networks, Electrical Power and Energy Systems 21 (1998) 269-277.

[8] A. Pleym, Connection of Distributed Generation—Effect on The Power System, Report of GodGunet Work Package 5, Norway, 2003, p. 115.

[9] D.W. Nowotny, T.A. Lipo, Vector Control and Dynamics of AC Drives, Oxford University Press, New York 1996, p. 440.

[10] J. Morren, S.W.H. Haan, Short-circuit current of wind turbines with doubly fed induction generator, IEEE Transactions on Energy Conversion 22 (1) (2007) 174-180.

[11] J. Machowski, J.W. Bialek, J.R. Bumby, Power System Dynamics and Stability, John Wiley & Sons, West Sussex, United Kingdom, 1997, p. 461.

[12] A.S. Mäkinen, O. Raipala, K. Mäki, S. Repo, H. Tuusa, Fault ride-through capability of full-power converter wind turbine, Journal of Energy and Power Engineering 4 (10) (2010) 17.

[13] R. Teodorescu, M. Liserre, P. Rodriguez, Grid Converters for Photovoltaic and Wind Power Systems, John Wiley & Sons, Ltd., West Sussex, United Kingdom, 2011, p. 416.

[14] R. Pena, J.C. Clare, G.M. Asher, Doubly fed induction generator using back-to-back PWM converters and its application to variable-speed wind-energy generation, IEE Proceedings—Electric Power Applications 143 (3) (1996) 231-241.

[15] D. Xiang, L. Ran, P.J. Tavner, S. Yang, Control of a doubly fed induction generator in a wind turbine during grid fault ride-through, IEEE Transactions on Energy Conversion 21 (3) (2006) 652-662.

[16] A.S. Mäkinen, H. Tuusa, Effect of transient flux compensation control on fault ride through of doubly fed induction generator wind turbine, in: International Conference on Renewable Energies and Power Quality, Las Palmas de Gran Canaria, 2011, p. 6.

[17] J. Lopez, E. Gubia, E. Olea, J. Ruiz, L. Marroyu, Ride through of wind turbines with doubly fed induction generator under symmetrical voltage dips, IEEE Transactions on Industrial Electronics 56 (10) (2009) 4246-4254.

[18] A.S. Mäkinen, O. Raipala, S. Repo, H. Tuusa, Influence of reactive current injection during a voltage dip on the operation of wind turbine circuit breaker, in: IEEE 8th International Conference on Power Electronics, Jeju, South Korea 2011, p. 8.

[19] IEEE Guide for Automatic Reclosing of Line Circuit Breakers for AC Distribution and Transmission Lines, IEEE STD, IEEE Power Engineering Society, C37.104™-2002. 2003, p. 55.

[20] O. Rintamäki, K. Kauhaniemi, Applying modern communication technology to loss-of-mains protection, in: 20th International Conference on Electricity Distribution, Prague, 2009, p. 4.

[21] S. Conti, Analysis of distribution network protection issues in presence of dispersed generation, Electric Power System Research 79 (2009) 49-56.